



ZEB2, a master regulator of the epithelial–mesenchymal transition, mediates trophoblast differentiation[†]

Sonia C. DaSilva-Arnold ^{1,2}, Che-Ying Kuo^{4,5,6}, Viralkumar Davra³, Yvonne Remache¹, Peter C.W. Kim⁶, John P. Fisher^{4,5,6}, Stacy Zamudio¹, Abdulla Al-Khan¹, Raymond B. Birge³, and Nicholas P. Illsley ^{1,*}

¹Department of Obstetrics and Gynecology, Division of Maternal Fetal Medicine and Surgery and Center for Abnormal Placentation, Hackensack University Medical Center, Hackensack, NJ, USA ²Department of Cell Biology and Molecular Medicine, Rutgers New Jersey Medical School, Newark, NJ, USA ³Department of Microbiology, Biochemistry and Molecular Biology, Rutgers New Jersey Medical School, Newark, NJ, USA ⁴Fischell Department of Bioengineering, University of Maryland, College Park, MD, USA ⁵NIH Center for Engineering Complex Tissues, University of Maryland, College Park, MD, USA ⁶Sheikh Zayed Institute for Pediatric Surgical Innovation, Children's National Health System, Washington DC, USA

*Correspondence address. Department of Obstetrics and Gynecology, 30 Prospect Ave, Hackensack, NJ 07601, USA. Tel: +1-551-996-8122; Fax: +1-551-996-8322; E-mail: nicholas.illsley@hackensackmeridian.org  orcid.org/0000-0002-4336-2832

Submitted on July 11, 2018; resubmitted on October 9, 2018; editorial decision on November 19, 2018; accepted on November 20, 2018

STUDY QUESTION: Does the upregulation of the zinc finger E-box binding homeobox 2 (*ZEB2*) transcription factor in human trophoblast cells lead to alterations in gene expression consistent with an epithelial–mesenchymal transition (EMT) and a consequent increase in invasiveness?

SUMMARY ANSWER: Overexpression of *ZEB2* results in an epithelial–mesenchymal shift in gene expression accompanied by a substantial increase in the invasive capacity of human trophoblast cells.

WHAT IS KNOWN ALREADY: *In-vivo* results have shown that cytotrophoblast differentiation into extravillous trophoblast involves an epithelial–mesenchymal transition. The only EMT master regulatory factor which shows changes consistent with extravillous trophoblast EMT status and invasive capacity is the *ZEB2* transcription factor.

STUDY DESIGN, SIZE, DURATION: This study is a mechanistic investigation of the role of *ZEB2* in trophoblast differentiation. We generated stable *ZEB2* overexpression clones using the epithelial BeWo and JEG3 choriocarcinoma lines. Using these clones, we investigated the effects of *ZEB2* overexpression on the expression of EMT-associated genes and proteins, cell morphology and invasive capability.

PARTICIPANTS/MATERIALS, SETTING, METHODS: We used lentiviral transduction to overexpress *ZEB2* in BeWo and JEG3 cells. Stable clones were selected based on *ZEB2* expression and morphology. A PCR array of EMT-associated genes was used to probe gene expression. Protein measurements were performed by western blotting. Gain-of-function was assessed by quantitatively measuring cell invasion rates using a Transwell assay, a 3D bioprinted placenta model and the xCelligenceTM platform.

MAIN RESULTS AND THE ROLE OF CHANCE: The four selected clones (2 × BeWo, 2 × JEG3, based on *ZEB2* expression and morphology) all showed gene expression changes indicative of an EMT. The two clones (1 × BeWo, 1 × JEG3) showing >40-fold increase in *ZEB2* expression also displayed increased *ZEB2* protein; the others, with increases in *ZEB2* expression <14-fold did not. The two high *ZEB2*-expressing clones demonstrated robust increases in invasive capacity, as assessed by three types of invasion assay. These data identify *ZEB2*-mediated transcription as a key mechanism transforming the epithelial-like trophoblast into cells with a mesenchymal, invasive phenotype.

LARGE SCALE DATA: PCR array data have been deposited in the GEO database under accession number GSE116532.

LIMITATIONS, REASONS FOR CAUTION: These are *in-vitro* studies using choriocarcinoma cells and so the results should be interpreted in view of these limitations. Nevertheless, the data are consistent with *in-vivo* findings and are replicated in two different cell lines.

[†]Presented in part at the International Federation of Placenta Associations, September 2017, Manchester, United Kingdom.

WIDER IMPLICATIONS OF THE FINDINGS: The combination of these data with the *in-vivo* findings clearly identify ZEB2-mediated EMT as the mechanism for cytotrophoblast differentiation into extravillous trophoblast. Having characterized these cellular mechanisms, it will now be possible to identify the intracellular and extracellular regulatory components which control ZEB2 and trophoblast differentiation. It will also be possible to identify the aberrant factors which alter differentiation in invasive pathologies such as preeclampsia and abnormally invasive placenta (AKA accreta, increta, percreta).

STUDY FUNDING AND COMPETING INTEREST(S): Funding was provided by the Department of Obstetrics and Gynecology, Division of Maternal-Fetal Medicine and Surgery at Hackensack Meridian Health, Hackensack, NJ. The 3D bioprinted placental model work done in Drs Kim and Fisher's labs was supported by the Children's National Medical Center. The xCELLigence work done in Dr Birge's lab was supported by NIH CA165077. The authors declare no competing interests.

Key words: ZEB2 / BeWo / JEG3 / trophoblast / epithelial–mesenchymal transition / invasion

Introduction

Normal placental development is critical for a successful pregnancy and it relies, in part, on the well-orchestrated differentiation of the fetal-derived trophoblast cell lineage into either the epithelial barrier layer of the placenta, the syncytiotrophoblast, or the invasive extravillous trophoblast (EVT). In the latter case, proliferative cytotrophoblast (CTB) cells located in the anchoring cell columns of the placenta differentiate into EVT, which invade the uterus and remodel the maternal spiral arterioles into large diameter, low resistance vessels capable of high-volume blood flow. EVT-mediated conversion of spiral arterioles is so integral to normal human placentation, that aberrant trophoblast invasion has been described as a key component of several major placental pathologies. These include trophoblast under-invasion, which can result in preeclampsia or intrauterine growth restriction (Naicker et al., 2003), as well as the converse, over-invasion, which can result in placenta accreta-related pathologies (abnormally invasive placenta, AIP) (Tantbirojn et al., 2008). In fact, the more severe forms of AIP (increta, percreta) are characterized by unusually deep trophoblast invasion with remodelling of the deeper myometrial blood vessels that feed into the spiral arteries, often resulting in substantial haemorrhage during delivery (Khong and Robertson, 1987; Tantbirojn et al., 2008).

The mechanism underlying trophoblast differentiation into the invasive EVT remains elusive. However, we (DaSilva-Arnold et al., 2015, 2018) and others (Pijnenborg et al., 1980; Vicovac and Aplin, 1996; Kokkinos et al., 2010), have suggested that the differentiation of CTB into EVT involves a regulated epithelial–mesenchymal transition (EMT), a highly conserved molecular process similar to that seen in embryogenesis, wound healing and in pathological conditions, e.g. cancer metastasis. All EMT types share common features, e.g. the transformation of polarized, anchorage-dependent epithelial cells into highly invasive, anchorage-independent cells (Greenburg and Hay, 1982). Although CTB differentiation to EVT shares some features with the three well-defined EMT types, there are significant differences (Kalluri and Weinberg, 2009). Unlike embryogenesis (Type I EMT), CTB differentiation does not generate the mesenchyme of a new tissue. Nor does it appear to have the mobility and flexibility to regenerate epithelial cells, unlike cancer metastasis (Type 3 EMT). Like carcinomas however, EVT (the differentiated CTB) have a degree of plasticity characterized by the simultaneous retention of epithelial traits while acquiring mesenchymal features (Kalluri and Weinberg, 2009; DaSilva-Arnold et al., 2015, 2018). We recently reported that third trimester EVT also have some plasticity; specifically, in the third trimester of

pregnancy, the EMT process is scaled back when compared to the first trimester, resulting in EVT that are in a metastable, less mesenchymal state compared to first trimester EVT. Conversely, our evidence also supports that third trimester EVT from over-invasive AIP pathologies demonstrate a more mesenchymal EMT status compared to normal third trimester EVT (DaSilva-Arnold et al., 2018).

A variety of signalling pathways are capable of promoting EMT, but they converge on a few key transcription factors that act as the master regulators of this process, including *GSC*, *SNAI1*, *SNAI2*, *TWIST1*, *ZEB1* and *ZEB2* (zinc finger E-box binding protein 2; previously known as SMAD-interacting protein 1, *SIP1*) (Comijn et al., 2001; Eger et al., 2005). Our previous work indicated that *ZEB2* is expressed at a level ~200-fold higher in the invasive first trimester EVT compared to CTB (DaSilva-Arnold et al., 2015). We also noted that *ZEB2* levels were substantially down-regulated in third trimester EVT, concurrent with the loss of invasive capacity (DaSilva-Arnold et al., 2018). These results and the absence of significant changes in the other master regulators raised the possibility that *ZEB2* is the key mediator of the EMT process in trophoblast differentiation. In this study, our aim was to test the mechanistic role of *ZEB2* in CTB to EVT differentiation. We hypothesized that upregulation of *ZEB2* in epithelial trophoblast would induce gene expression and phenotypic alterations consistent with an epithelial–mesenchymal progression and with a subsequent increase in invasiveness. We used an *in-vitro* approach to overexpress *ZEB2* in two epithelial trophoblast models, BeWo and JEG3 choriocarcinoma cells, to study EMT-associated gene expression and invasiveness.

Materials and Methods

Cell culture and generation of stable cell lines

Human-derived BeWo cells (b30 clone, courtesy of Dr Kenneth Audus, University of Kansas) and JEG3 cells (a gift from Dr William Ackerman III, The Ohio State University) were cultured in DMEM/F12 (1:1) (Hyclone Laboratories Inc., Logan, UT) supplemented with 10% Fetal Bovine Serum (FBS; Atlanta Biologicals, Flowery Branch, GA), GlutaMAX (Gibco, Gaithersburg, MD), and 1% penicillin-streptomycin (P/S; Gibco). HTR-8/SVneo cells (a gift from Dr Charles Graham, Queen's University, Canada) were cultured in RPMI-1640 (Gibco) supplemented with 5% FBS, GlutaMAX and P/S. Prior to commencing our studies, we confirmed the identity of all cell lines, BeWo, JEG3 and HTR-8/SVneo, using a human genetic 9-marker STR Profile (CellCheck 9; IDEXX BioResearch, Westbrook, ME). All cells were

shown to be free from mycoplasma contamination using the MycoAlert Plus Detection kit (Lonza, Walkersville, MD) and passaged under aseptic conditions. Unless otherwise stated, all cell lines were grown to, and analysed at ~60% confluency and were used before passage number 30 (HTR-8/SVneo: under passage 90). All cultures were maintained at 37°C in a humidified incubator with a 5% CO₂ atmosphere.

Competent *E. coli* DH5 α cells (Invitrogen, Carlsbad, CA) were transformed with either an empty vector (*pRECEIVER-Lv225-hNEG-GFP*) or a *ZEB2* open reading frame (ORF) expression construct with an EF1A promoter region, green fluorescent protein (GFP), and a puromycin resistance element (*pRECEIVER-Lv225-hZEB2-GFP*; NM_014795.3; GeneCopoeia, Rockville, MD) according to the manufacturer's protocol. The bacterial suspension was cultured overnight on LB plates with 100 μ g/ml carbenicillin (Teknova, Hollister, CA) and a colony was selected for plasmid purification with the plasmid endo-free Maxi kit (Qiagen, Valencia, CA). Lentiviral vectors were generated by transient transfection of each plasmid construct (10 μ g DNA) with 10 μ g third-generation lentiviral packaging system (Applied Biological Materials, British Columbia, Canada) using the TurboFect transfection reagent (Pierce Biotechnology, Rockford, IL), into HEK293T cells, according to the manufacturer's instructions. Lentivirus-containing supernatants were harvested at 72- and 96-h post-transfection, cleared by low-speed centrifugation, and filtered through a 0.45 μ m pore size PES low protein-binding filter. The supernatant was stored at -80°C in single-use aliquots to be used for lentiviral titering and stable clone generation. The viral nucleic acid content was quantified using the QuickTiter Lentivirus Titer kit (Cell Biolabs, San Diego, CA). Both BeWo and JEG3 cells were infected with either empty vector (EV) or *ZEB2*-expressing lentivirus (MOI = 10) in the presence of 8 μ g/ml polybrene. Following transduction, *ZEB2*-expressing cells were selected and subsequently maintained in 4 μ g/ml puromycin. To generate stable *ZEB2*-expressing clonal cell lines, the highest GFP-expressing cells were sorted on a FACSAria II flow cytometer (BD Biosciences, San Jose, CA) based on the fluorescence produced from GFP in the overexpression vector. Single, high GFP-expressing cells were cultured separately in 96-well plates and stable clonal cell lines were developed from these cultures. The stable clones were expanded and gene expression was quantified by extracting total RNA for quantitative RT-PCR (qRT-PCR) using primers specific to human *ZEB2* (Hs00207691_m1; Taqman Gene Expression Assays; Applied Biosystems, Foster City, CA) and normalized to a housekeeping gene, *YWHAZ* (Hs03044281_g1) using the $\Delta\Delta C_T$ method (Livak and Schmittgen, 2001). Two BeWo clones (c6/f11) and two JEG3 clones (a7/b5) were chosen for downstream analysis of gene expression, protein expression and functional invasiveness based on their *ZEB2* expression and morphology. EV clones were expanded as a mixed colony and maintained in puromycin.

RNA isolation and PCR array

All cells utilized for analysis on a PCR array were plated as monolayers in 24-well plates to reach ~40–60% confluency after 24 h. Cells were washed twice with PBS and extracted directly into QIAzol (Qiagen, Valencia, CA). Genomic DNA was enzymatically digested by DNase I treatment and total RNA was captured by column purification using the miRNeasy Micro kit (Qiagen) according to the manufacturer's

instructions. Both RNA concentration and integrity were quantified on an RNA 6000 Nano Chip using the Agilent 2100 Bioanalyzer (Agilent Technologies, Santa Clara, CA). All samples were reverse transcribed from 200 ng total RNA to cDNA using the SuperScript III First Strand Synthesis System (Invitrogen, Carlsbad, CA). Samples were analysed with the Epithelial–Mesenchymal Transition (EMT) RT² Profiler PCR array (Cat #PAHS-090_ZC, Qiagen) on an ABI 7900 HT Fast Real-Time PCR System (Applied Biosystems, Foster City, CA) as previously described (DaSilva-Arnold *et al.*, 2015, 2018). The 2^(- $\Delta\Delta C_T$) method was used to obtain the fold-change in relative gene expression between each BeWo clone (BeWo_c6 and BeWo_f11) and BeWo empty vector (BeWo_EV) normalized to four housekeeping genes (GAPDH, RPLP0, B2M, and ACTN). Similarly, each JEG3 clone (JEG3_b5 and JEG3_a7) was compared to the JEG3 empty vector clone (JEG3_EV) normalized to three housekeeping genes (GAPDH, RPLP0 and HPRT1). The data is presented as the mean \pm SEM of three independent experiments.

Cell morphology characterization

Morphological differences between *ZEB2*-transfected and EV clones were analysed from cells plated as monolayers prior to extraction for RNA. Phase-contrast images were recorded at 10X with a Nikon Eclipse TS100 (Nikon Instruments, Melville, NY) with a QICAM digital camera loaded with QCapture v.2.68.2 (QImaging, British Columbia, Canada). The shape was quantified using ImageJ software (v1.53, NIH). The cell aspect ratio was calculated by dividing the length of a cell's major axis by the width of the minor axis. Approximately 20–30 cells per image present at the periphery of a colony were recorded. All data are presented as the mean \pm SD of four independent images per cell type.

Immunofluorescent staining

All cells stained with immunofluorescent antibodies were plated as monolayers in glass chamber slides (Nalgen Nunc, Rochester, NY) to reach ~40–60% confluency after 24 h. The cells were fixed and permeabilized with ice-cold acetone for 10 min, then washed three times in PBS. Non-specific binding was blocked with BlockAid (Thermo Scientific) in 0.1% Tween for 1 h at room temperature. Immunolabeling was performed with primary antibodies in a humidified chamber overnight at 4°C; primary antibodies comprised mouse monoclonal anti-occludin Alexa Fluor 488 (1:40; clone OC-3F10, Thermo Scientific) or rabbit polyclonal anti-E-Cadherin (1:100; clone C1C3, GeneTex). Following incubation with primary antibodies, slides with E-cadherin were washed three times with PBS and incubated with Alexa Fluor 488-labelled anti-rabbit IgG in BlockAid (1:500; Molecular Probes) for 30 min at room temperature and washed three times with PBS. In all slides, the nuclei were counterstained with Hoechst 33342 (Invitrogen) for 5 min at room temperature and washed three times with PBS. Slides were air-dried and cover-slipped with ProLong Anti-Fade (Thermo Scientific). Images were acquired at the same exposure with the Nikon AIR confocal microscope and merged with NIS Elements AR 5.02 software (Nikon Instruments).

Western blotting

Total protein expression of BeWo and JEG3 cells was analysed from parental, EV and stable *ZEB2* clones plated as monolayers in 6-well

plates. After reaching ~40–60% confluency, cells were washed twice in cold PBS, and total protein was extracted into RIPA buffer containing 0.1% CHAPS and processed as previously described (DaSilva-Arnold et al., 2018). Briefly, after determining the protein content by BCA assay (Pierce Biotechnology), 25 µg of total protein per sample was separated on 8–16% SDS-PAGE gels and transferred to a nitrocellulose membrane. Immunoblotting was performed by overnight incubation with primary antibodies diluted in PBS containing 3% BSA at 4°C. The primary antibodies used (see Supplementary Table I) were the rabbit polyclonal antibodies: anti-cytokeratin-7 (1:1000; clone N1C2; GeneTex, Irvine, CA), anti-E-cadherin (1:500; GeneTex), anti-IGFBP4 (1:1000; R&D Systems), anti-matrix metalloproteinase-2 (MMP-2; 1:1000; GeneTex), anti-N-cadherin (1:1000; GeneTex) anti-vimentin (1:1000; Abcam) and anti-ZEB2 (1:1000; Thermo Scientific). Mouse monoclonal antibodies included: anti-cytokeratin 14 (1:1000; clone LL02, Bio-Rad), anti-fibronectin-I (1:1000; clone 10/Fibronectin, BD Bioscience, San Diego, CA), anti-HLA-G (1:500; clone MEM-G/4, Thermo Scientific) and anti-matrix metalloproteinase-9 (1:1000; clone EPI255Y, Abcam). The membranes were re probed with anti-β-actin (1:2000; clone AC15; Sigma-Aldrich, St. Louis, MO) as loading control. Images were visualized with the Trident Plus Chemiluminescence kit per manufacturer's instructions (GeneTex) on a ChemiDoc MP Imager (Bio-Rad Laboratories, Hercules, CA) and quantified using ImageJ software (v1.53, NIH). All data are presented as the mean ± SD of three independent experiments performed in triplicate.

Invasion (Transwell) assay

The BeWo and JEG3 choriocarcinoma cell lines were analysed for migration and invasion on thin Matrigel-coated or thick Matrigel-coated polycarbonate membrane (8-µm pore size) Transwell inserts (Corning Inc, Corning, NY) as described by Justus et al. (2014) with minor modifications. BeWo or JEG3 cells were grown to ~60% confluency and passaged at a 1:2 dilution 24-h before serum starvation. For cell invasion, the Transwell inserts in a 24-well plate format were coated with Matrigel® Basement Membrane Matrix, LDEV-free (Corning Inc) dissolved in 100 µl of serum-free medium (DMEM, high glucose, no calcium, supplemented with 4 mM GlutaMAX) at 0.3 mg/ml (BeWo) or 0.5 mg/ml (JEG3 and HTR-8/SVneo) concentrations under aseptic conditions. A thin Matrigel-coated insert was also prepared as a migration control to enable determination of the rate of cell invasion for each cell line (0.03 mg/ml for BeWo or 0.05 mg/ml for JEG3 and HTR-8/SVneo). The Matrigel-coated inserts were allowed to gel for ~3 h at room temperature, then placed in an incubator at 37°C prior to use. Concurrently, BeWo or JEG3 (EV and ZEB2 clones) were washed with PBS and starved in low serum conditions (0.5% FBS) for 6 h in DMEM, high glucose, no calcium, supplemented with 4 mM GlutaMAX, and HTR-8/SVneo in RPMI 1640 containing 0.5% FBS. At the given time for seeding, cells were enzymatically dissociated with Accutase (STEMCELL Technologies, Cambridge, MA), washed with PBS to remove serum, and resuspended in DMEM, high glucose, without calcium for BeWo and JEG3 (or RPMI for HTR-8/SVneo) with 0.5% FBS. A seeding density of 5.0×10^4 cells per well was placed in the upper chamber while a chemoattractant (10% FBS) was added to the lower chamber in the same medium. The plates were incubated at 37°C for 24 h (JEG3) or 48 h (BeWo). HTR-8/SVneo were assayed in

parallel with the BeWo and JEG3 cells. When being compared to BeWo invasion over 48 h, the HTR8/SVneo were plated at a lower seeding density (2.0×10^4 cells/well). At the designated endpoint, the migrated/invaded cells were fixed with 4% paraformaldehyde (10 min), washed with PBS, and stained with hematoxylin and eosin (H&E). The cells on the seeding side of the membrane (upper chamber) were gently removed with a cotton-tip applicator and the membranes were cut and positioned in 50% glycerol: 50% PBS on coverslips. Images of the H&E stained cells that attached to the reverse side of each filter were taken for three random non-overlapping fields at 100X with a Nikon Eclipse TS100 inverted microscope (Nikon Instruments). Cell invasiveness was expressed as the ratio of each cell line invading through the thick Matrigel and normalized to the number of cells migrating through thin Matrigel for each cell type (expressed as mean % invasion). All data are presented as the mean ± SEM of a minimum of three independent experiments performed in triplicate.

Real-time monitoring using the RTCA DP xCELLigence system

Real-time migration and invasion of BeWo and JEG3 cell lines was analysed using CIM-16 plates on the RTCA DP xCELLigence system (ACEA Biosciences, San Diego, CA) per manufacturer's instructions. BeWo or JEG3 cell lines were grown to ~60% confluency and passaged at a 1:2 dilution 24-h before serum starvation. The cells were washed with PBS and starved in 1% FBS-containing medium for 8 h in each cell line's respective medium as described above (cell culture). The upper chamber of the CIM-plates was coated with 50 µg/ml or 500 µg/ml of Matrigel (Corning Inc) for cell migration and invasion assays respectively and placed in a 37°C incubator for 4 h. Medium containing 10% FBS was used as a chemoattractant in the bottom chamber of the CIM-16 plate. The cells were detached using Accutase and resuspended in the respective medium containing 1% FBS and 100 ng/ml human epidermal growth factor (EGF) to the final concentration of 4×10^5 cells/ml. Cells were seeded (4×10^4 cells) in triplicate to wells in the top chamber. Invasiveness as indicated by the change in the cell index versus time was measured every 10 min for 72-h and graphed as the Δ cell index from at least four wells ± SD.

Measurement of invasion using a 3D bioengineered placenta model (3D-BPM)

BeWo and JEG3 choriocarcinoma cell invasion was measured using a novel 3D-BPM as previously published, using gelatin-methacrylate (gelMA) discs (Kuo et al., 2016, 2018a, 2018b). All bioprinting was done on a commercial 3D bioprinter (3D-Bioplotter; EnvisionTEC, Dearborn, MI) using a prepolymer solution prepared from the gelMA. Cells were bioprinted (2 million cells/ml) in gelMA/growth medium with low serum (5% FBS) along the periphery of the cylindrical placental model (height = 2 mm, diameter = 10 mm) with a chemoattractant (EGF, 10 µM) at the centre. Phase-contrast images were taken on Days 2 and 7 with an inverted microscope (Olympus CKX42). Invasion rates were determined by measuring the average distance between the edge of the placental model construct and the invasion front using an inverted fluorescent microscope (Olympus) at different time points (Day 1 vs. Day 8). All data are presented as the mean ± SEM of experiments done in triplicate.

Statistics

Statistical analyses were conducted and plotted using GraphPad Prism 7.03 (GraphPad Software, LaJolla, CA). D'Agostino-Pearson/Shapiro-Wilk's and Levene's tests were used to test for normality and equal variance of the data, respectively. Significance between groups for the cell aspect ratio did not satisfy normality; therefore, the Mann-Whitney *U* test was used. For the PCR arrays, the statistical significance between each clone and its respective empty vector control was determined from the $2^{(-\Delta\text{CT})}$ values by one-way ANOVA using Tukey's multiple comparison test when normality and equal variance assumptions were met, or for the non-parametric, Kruskal-Wallis analysis with a Dunn's multiple comparison test. The Transwell invasion assays did not satisfy normality, so the differences were calculated using a Kruskal-Wallis test with significance determined by Dunn's multiple comparison test. Western blotting was tested using one-way ANOVA employing a Brown-Forsythe test with a Tukey's analysis when normality was met, or alternatively a Kruskal-Wallis analysis with a Dunn's multiple comparison test. Results are shown as standard error of the mean (SEM), unless otherwise indicated, when three independent experiments were conducted. Statistical significance was assigned as *P*-value < 0.05.

Results

Generation and choice of stable *ZEB2* overexpression clone cells

We generated stable clones of BeWo and JEG3 cells with an expression vector containing the *ZEB2* coding region and two selection markers, coding for GFP and puromycin resistance. Multiple *ZEB2* overexpression clones (*ZEB2*^{oe}) were generated, each originating from a single cell that was isolated by FACS from the top 1% of GFP-expressing cells. We initially analysed various clones using Taqman qRT-PCR to measure *ZEB2* expression change compared to the parental cells. Figure 1A shows the data for the representative clones which we selected from each cell line (BeWo_c6, BeWo_f11; JEG3_b5, JEG3_a7) that reflected increased *ZEB2* gene expression. Thus, *ZEB2* expression in the BeWo_f11 clone was ~95-fold that of the BeWo parental line, while BeWo_c6 was greater than 300-fold higher than the parental cells. *ZEB2* expression in the JEG3_a7 clone was ~300-fold higher than the JEG3 parental cells and JEG3_b5 expression was greater than 500-fold higher. All the selected *ZEB2*^{oe} clones showed levels of *ZEB2* closer to that demonstrated for the EVT model cell line, HTR8/SVneo (~400-fold > BeWo parental cells). Prior to any further analyses, the gene expression of both BeWo and JEG3 parental cells were compared to their respective empty vector controls (BeWo_EV and JEG3_EV) and found to be not significant (*P* = 0.99). It should be noted that the *C_T* values for the BeWo and JEG3 parental cells were in the range 32–36, demonstrating a very low level of expression, thus the high values for the overexpressing clones are due in part to a very low denominator.

In addition to the aforementioned qRT-PCR, RNA from *ZEB2*-expressing cells was also measured as part of the EMT PCR array. The *ZEB2* expression changes determined from the PCR array measurements differed substantially from those measured by Taqman qRT-PCR assay. Nevertheless, it is important to note that the same

relationship was maintained whether gene expression was measured by Taqman assay or by PCR array, e.g. that *ZEB2* expression in the high expression clones (BeWo_c6, JEG3_b5) is 3–4-fold greater than that in the lower expressing clones (BeWo_f11, JEG3_a7). Using the PCR array, we measured the difference between the empty vector controls (BeWo_EV, JEG3_EV) and the *ZEB2*^{oe} clones. Compared to the BeWo_EV control, the PCR array indicated a 44.4 ± 1.3 -fold upregulation (*n* = 3, *P* = 0.011) for the BeWo_c6 and a 13.9 ± 4.9 -fold increase for the BeWo_f11, (*n* = 3; NS). Compared to the JEG3_EV control, *ZEB2* expression in JEG3_b5 was increased 40.3 ± 12.8 -fold (*n* = 3, *P* = 0.026) and in JEG3_a7, by 9.3 ± 3.9 -fold (*n* = 3; NS). Clearly the level of gene expression measured in the PCR array is substantially lower than that in the Taqman measurements shown in Fig. 1A. There are multiple reasons for the differences between the assay methods (e.g. Taqman vs. SYBR Green assay methods, differing primers), however since we were assessing changes in other EMT-associated genes using the PCR array, we elected, hereafter, to utilize the values of *ZEB2* expression observed in the PCR array.

Overexpression of *ZEB2* was verified by western immunoblot of total cell lysates. The results are shown in Fig. 1B and C, comparing protein expression in the parental cells, the EV controls and the *ZEB2*^{oe} clones for both BeWo and JEG3. The BeWo_c6 clone showed a higher expression of *ZEB2* protein (*n* = 3; *P* = 0.003) compared to the BeWo_EV control. Similarly, the JEG3_b5 clone had increased *ZEB2* protein (*n* = 3; *P* = 0.037) compared to the JEG3_EV control. In both cases, the *ZEB2* mRNA upregulation is reflected in increased *ZEB2* protein. However, this was not evident with the BeWo_f11 or JEG3_a7 clones, where the lesser increase in *ZEB2* mRNA did not translate into significantly increased *ZEB2* protein.

Morphological alterations in stable *ZEB2*^{oe} clones suggest EMT

Following clone generation, we compared the morphology of the high *ZEB2*-expressing clone cells to the parental (par) cell lines and to the empty vector (EV) controls. The morphological comparisons of the cells indicated that our *ZEB2*^{oe} clones had a transitional appearance, between the parental (non-transduced) BeWo and JEG3 cells and the EVT-like model cell line, HTR-8/SVneo. Both high *ZEB2*-expressing stable clones have a loss of cell-cell junctions (Fig. 2A, B, Supplementary Fig. 1) and a gain of an elongated structure characteristic of mesenchymal-like cells. This change was quantified as the cell aspect ratio (ratio of the length of the major axis to the width of the minor axis) and is shown to be increased in *ZEB2*^{oe} BeWo clone compared to EV control (BeWo_EV, 1.63 ± 0.35 ; BeWo_c6, 2.46 ± 0.82 , *P* < 0.0001; Fig. 2C). The same is true of the *ZEB2*^{oe} JEG3 clone compared to control (JEG3_EV, 1.65 ± 0.38 ; JEG3_b5, 2.31 ± 0.79 , *P* < 0.0001; Fig. 2C). The BeWo and JEG3 cells transduced with EV were phenotypically similar to the parental cell lines (Fig. 2A, B).

Gene expression of stable *ZEB2*^{oe} clones indicate a shift to a mesenchymal pattern

RNA was extracted from all cell lines, BeWo and JEG3 parental, EV and *ZEB2*^{oe} stable clones, and analysed by an EMT-specific PCR array to identify gene expression changes as previously described (DaSilva-Arnold *et al.*, 2015, 2018). RNA integrity number (RIN) scores were uniformly ≥ 9 indicating high-quality RNA (Schroeder *et al.*, 2006). The

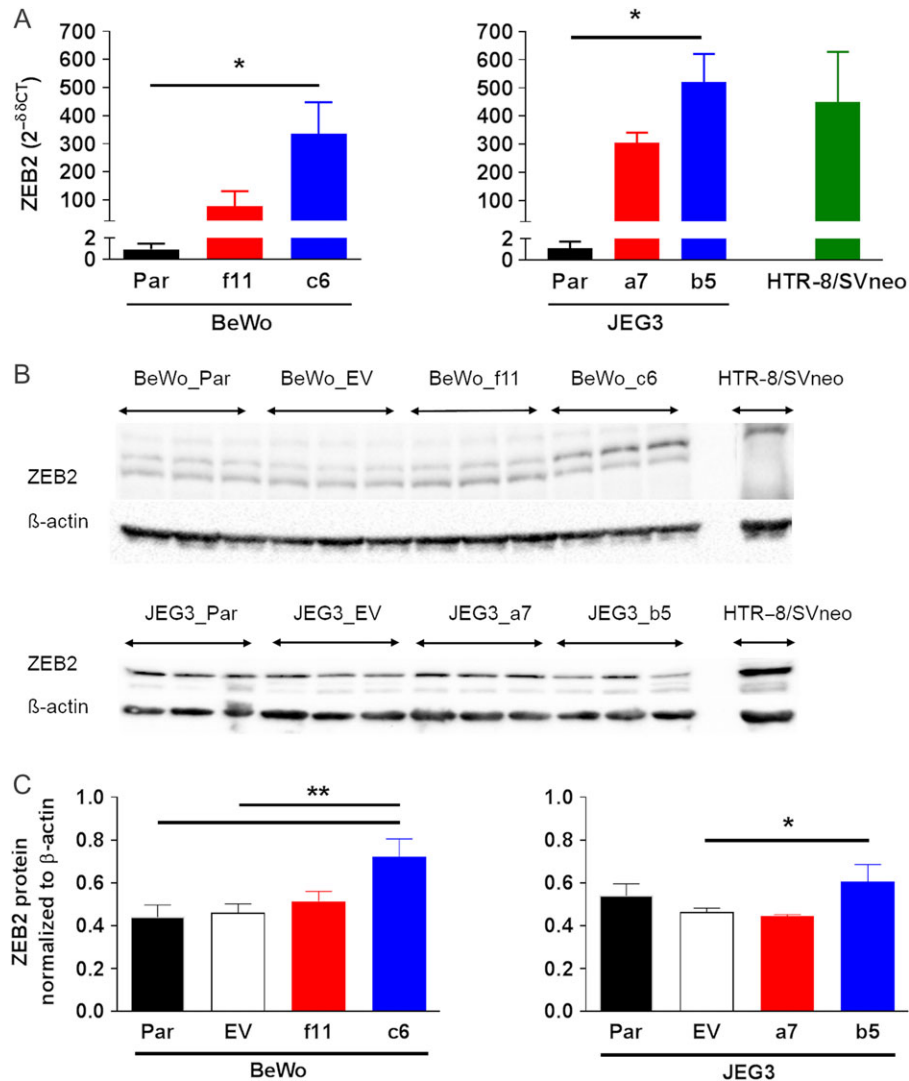


Figure 1 Validation of *ZEB2* overexpression in authenticated trophoblast cell lines. Quantitative RT-PCR and western blot of *ZEB2* expression in BeWo and JEG3 stable clones was performed to select clones for downstream analyses, ultimately selecting BeWo_c6 and JEG3_b5 for downstream functional changes. **(A)** Gene expression of BeWo and JEG3 clones was compared to each parental cell line by Taqman qRT-PCR. BeWo_c6, JEG3_a7 and JEG3_b5 clones express increased *ZEB2* mRNA compared to parental cells (Kruskal–Wallis with Dunn’s multiple comparisons, * $P < 0.05$). Results are the mean \pm SEM of three independent experiments performed in triplicate. **(B and C)** Total protein expression of BeWo, JEG3 and HTR-8/SVneo was analysed by western blot. Quantification of protein expression shows that BeWo_c6 and JEG3_b5 have increased *ZEB2* protein compared to parental (Par) and empty vector (EV; ANOVA with Tukey’s multiple comparison test, * $P = 0.0365$, ** $P < 0.01$). Results are the mean \pm SD performed in triplicate.

graphical representation in Fig. 3A highlights the gene expression fold-change in the BeWo_c6 and BeWo_f11 *ZEB2*^{oe} clones ($n = 3$) compared to the EV control ($n = 3$). This comparison shows well-recognized alterations in EMT-related genes. Thus for the BeWo_c6 comparison to BeWo_EV control, this includes a loss of epithelial-associated genes involved in cell adhesion processes such as *DSP* (desmoplakin; -1.9 ± 0.05 , $P = 0.008$), *F1IR* (F11 receptor; -2.05 ± 0.09 , $P = 0.009$), *PLEK2* (pleckstrin 2; -2.62 ± 0.04 , $P < 0.001$) and *OCLN* (occludin; -2.2 ± 0.1 -fold, $P = 0.008$); the latter change is only seen in the BeWo_c6 clone. There is also loss of *BMP7* (bone morphogenic protein 7; -9.2 ± 0.1 , $P < 0.001$), a member of the TGF β superfamily previously shown to be involved in promoting the epithelial phenotype (Zeisberg et al., 2003;

Buijs et al., 2007; Naber et al., 2012; Duangkumpha et al., 2014). In addition, *ZEB2* overexpression in BeWo_c6 also leads to gain of mesenchymal markers such as *CAV2* (caveolin 2; 2.7 ± 0.1 , $P < 0.001$), *ERBB3* (ErbB2 Receptor tyrosine kinase 3; 3.4 ± 0.7 , $P = 0.025$), *SPARC* (secreted protein acidic and rich in cysteine; 6.7 ± 0.2 , $P = 0.021$) and *TGFBI* (transforming growth factor beta 1; 4.3 ± 0.7 , $P = 0.021$). Notable also are the increases in *MMP2* (matrix metalloproteinase 2; 9.5 ± 1.3 , $P = 0.016$) and *MMP9* (matrix metalloproteinase 9; 3.2 ± 0.3 , $P = 0.006$). The full complement of gene expression data for the BeWo_c6/BeWo_EV comparison is found in Supplementary Table II. Comparison of the second BeWo stable clone (BeWo_f11 to BeWo_EV control; Fig. 3A, Supplementary Table II) indicates some gene expression changes in

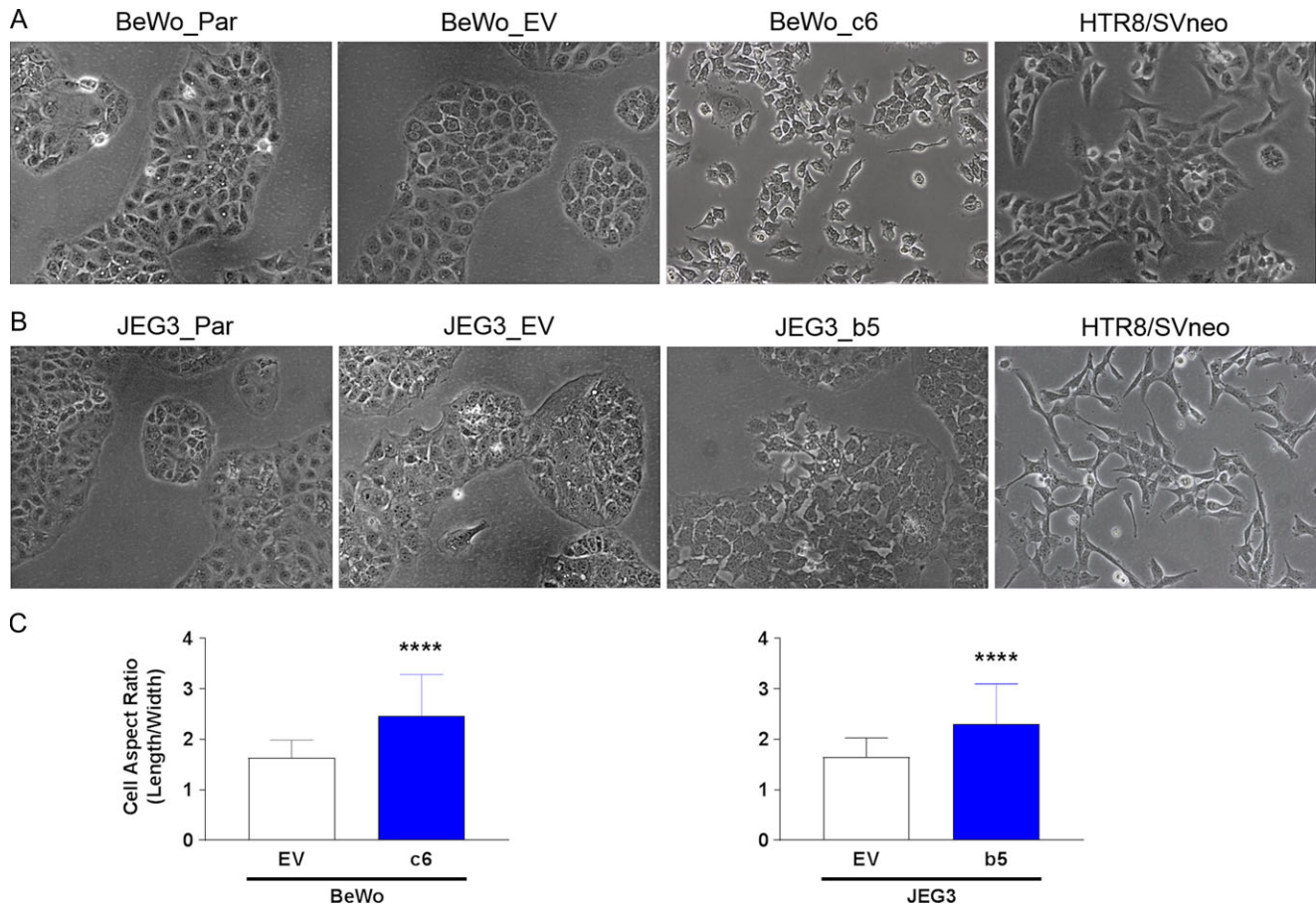


Figure 2 Demonstration of phenotypic changes representative of epithelial–mesenchymal transition (EMT). Two choriocarcinoma cell lines, **(A)** BeWo and **(B)** JEG3 were transduced with lentivirus containing a *ZEB2* overexpression vector and GFP, or GFP only (empty vector; EV) to produce stable clones. *ZEB2* BeWo and JEG3 stable clones have a loss of cell–cell junctions compared to the respective parental (Par) and EV cells. HTR-8/Svneo are representative of invasive extravillous trophoblast cells. **(C)** *ZEB2* overexpression results in a gain of an elongated structure in BeWo and JEG3 clones as measured by the cell aspect ratio (length of a cell’s major axis divided by the width of the minor axis; Mann Whitney, **** $P < 0.0001$). Approximately 20–30 cells per image present at the periphery of a colony were recorded. Results are the mean \pm SD of four independent images per cell type.

common with the BeWo_c6 clone; in some cases, differential expression is not as great as in the BeWo_c6. For example, in the BeWo_f11, the loss of *BMP7* is 5-fold less (-1.4 ± 0.1 , $P = 0.004$) than in BeWo_c6 (-9.2 ± 0.03 , $P < 0.001$). Nevertheless, there are some genes with significant changes in the BeWo_f11 that are not seen in BeWo_c6 including a loss in the epithelial marker *EGFR* (epidermal growth factor receptor; -2.5 ± 0.1 , $P = 0.048$) and an increase in the mesenchymal markers, *ITGB1* (integrin beta 1; 1.7 ± 0.04 , $P = 0.021$) and *VIM* (vimentin; 4.2 ± 0.9 , $P = 0.037$).

Although *ZEB2* expression is highly upregulated in the JEG3_b5 clone (Fig. 3B; Supplementary Table III), this clone displays a gene expression signature dissimilar to BeWo stable clones. In fact, the JEG3_b5 gene expression pattern shares few similarities with either of the BeWo clones. The high *ZEB2*-expressing JEG3_b5 clone does exhibit changes in several classical markers of the EMT, including *CDH2* (N-cadherin; 2.2 ± 0.3 ; $P = 0.008$), *ITGA5* (integrin alpha 5; 1.4 ± 0.04 ; $P = 0.001$), *ITGB1* (integrin beta 1; 1.5 ± 0.2 ; $P = 0.041$), and

other EMT master regulators *SNAI2* (Slug; 1.9 ± 0.2 , $P = 0.011$) and *TWIST1* (Twist; 3.44 ± 0.1 ; $P < 0.001$). Several gene expression changes are, however, opposite to those described for EMT in the literature (*CALD1*, -1.3 ± 0.02 ; $P = 0.001$; *FOXC2*, 3.5 ± 0.7 ; $P = 0.025$; *SNAI1*, -2.2 ± 0.1 ; $P = 0.008$). In the lower-expressing *ZEB2*^{oe} clone, JEG3_a7, there are approximately one-third fewer gene expression changes than the JEG3_b5 and, similar to the lower *ZEB2*^{oe} BeWo_f11 clone, the extent of the change generally appears to be lower (Fig. 3B; Supplementary Table III).

Notable also are the (cyto)keratins. These are generally regarded as epithelial markers, although there are numerous exceptions (see Discussion section). In the case of the *ZEB2*^{oe} BeWo clones, there are >2-fold increases in both *KRT7* and *KRT14*, while *KRT19* levels show no changes, compared to the EV control. In the case of the *ZEB2*^{oe} JEG3 clones, with exception of *KRT7* in JEG3_b5 (1.2-fold increase), there are no differences in cytokeratin expression compared to the EV control.

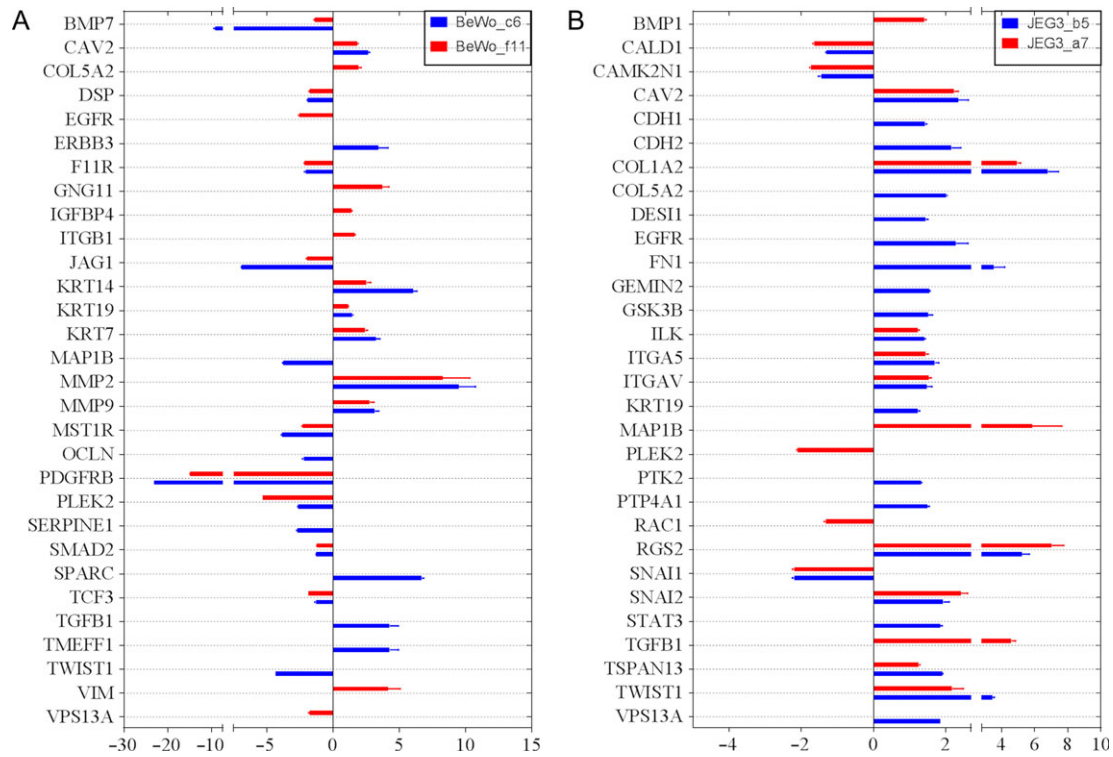


Figure 3 ZEB2 overexpressing stable clones show gene expression changes representative of an epithelial–mesenchymal transition. Two representative ZEB2 overexpressing (A) BeWo clones (c6/f1) and two (B) JEG3 clones (b5/a7) were selected for examination of the alterations in expression following ZEB2 qRT-PCR. Gene expression was measured using a PCR array for EMT-associated genes. The data is expressed as the relative fold-expression change between the overexpression clones and their respective empty vector controls (BeWo_EV or JEG3_EV; $P < 0.05$). The genes shown are those for which there was a significant change in expression for at least one of the two stable clones for each cell type. The data is presented as the mean \pm SEM of three independent experiments.

Stable ZEB2^{oe} clones have increased motility and invasion in Transwell assays

An integral feature of cells that undergo an EMT is an increase in the rates of migration and invasion. We used several approaches to assess whether ZEB2 upregulation is associated with increased migration and invasion. The first is a classic Transwell invasion assay. In the invasion assay, we employed a thick layer of Matrigel (300/500 $\mu\text{g}/\text{ml}$) which required cells to digest and invade into the extracellular matrix before traversing the Transwell. The presence of a Matrigel coating for both migration (thin coating) and invasion (thick coating) inserts ensured that differences in movement of cells across the insert was not due to differences in the extent of cell binding to the insert surface. BeWo are an epithelial-like trophoblast model cell line known to have the ability to fuse (a syncytiotrophoblast model) and have a very limited invasive potential (Lyden et al., 1993). However, after ZEB2 upregulation, our BeWo_c6 clone exhibited an enhanced chemotactic behaviour when cultured in calcium-free medium and was easily capable of passing through a thin-layer of Matrigel coating compared to BeWo_EV (Fig. 4A). This ZEB2 overexpression clone had substantially augmented invasiveness (mean percent invasion = $33.7 \pm 2.9\%$, $P = 0.0004$; Fig. 4B) through the thick Matrigel-coated insert compared to EV control ($13.2 \pm 1.9\%$). In fact, functionally, BeWo_c6 appeared to invade at a comparable rate to the EVT-like HTR-8/SVneo ($52.9 \pm 3.9\%$; $P =$

0.054). We should note that BeWo migration/invasion was assessed at 48-h, rather than 24-h, because the BeWo only appear to begin invading at the 24-h timepoint. This determination was made based on real-time monitoring of BeWo on the xCELLigence system (see below). On the other hand, JEG3, known to have invasive properties, was assayed at 24-h. The high ZEB2 expressing JEG3_b5 cells were able to invade through Matrigel at a greater rate compared to control (JEG3_EV, $15.3 \pm 2.3\%$ invasion rate; JEG3_b5, $40.2 \pm 9.1\%$; Fig. 4B).

Stable ZEB2^{oe} clones have increased invasion in two real-time assay systems: a novel 3D bioprinted placenta model (3D-BPM) and xCELLigence assays

Invasiveness was assessed by two other methods. The first of these utilized a novel 3D bioprinting technique (Kuo et al., 2016). The 3D-BPM is superior to 2D Transwell studies because it allows for real-time data acquisition of cell invasion in a system that simulates the three-dimensionality of the human placenta. A shell of cells is bioprinted in low serum conditions at the periphery of a gelatin methacrylate (gelMA) hydrogel disc which mimics an extracellular matrix (ECM) and contains fibronectin (model represented in Fig. 5A). As the cells degrade the ECM and travel towards the chemotactic factors

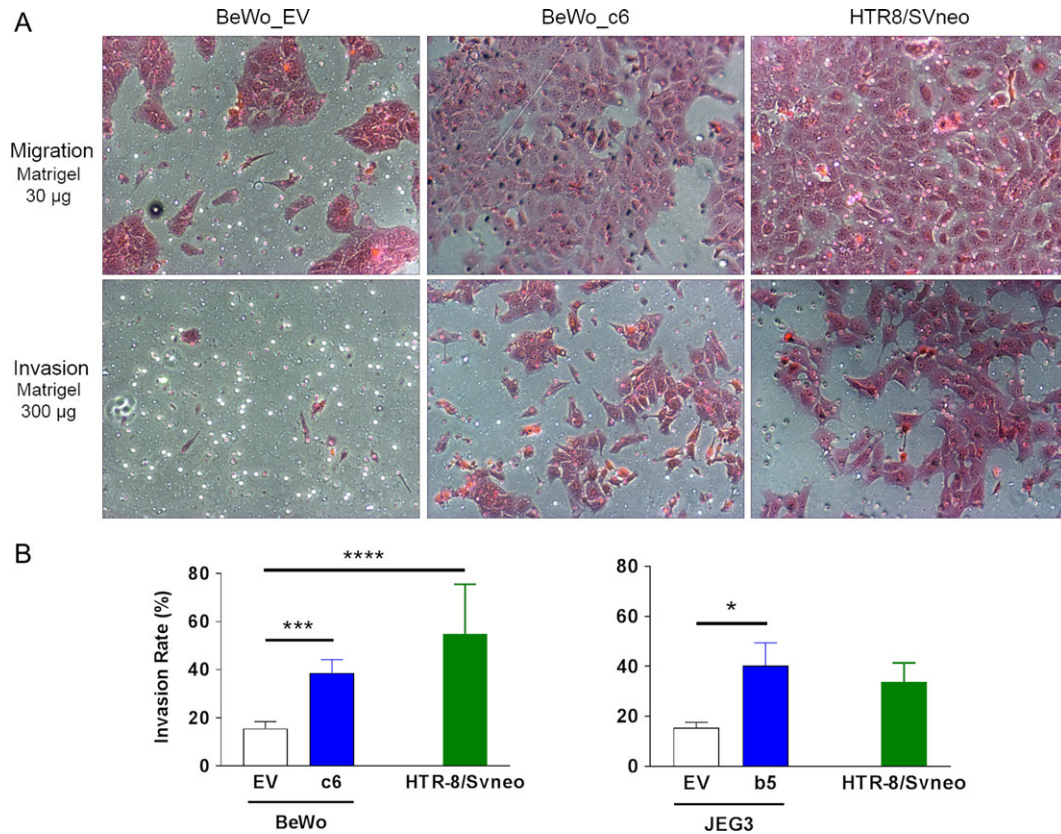


Figure 4 ZEB2 overexpression in trophoblast cell lines augments invasion through Transwell inserts. The invasion rate of BeWo and JEG3 clones (empty vector; EV or ZEB2 overexpression) was assessed on modified Boyden chambers (Transwell inserts) coated with Matrigel. (A) BeWo_EV, BeWo_c6, and HTR-8/SVneo were starved in low serum conditions (0.5% FBS) for 4–6 h and seeded on Transwell inserts (8- μ m pore size). All cells were H&E stained at 48-h, and (B) the ratio of cells able to invade (thick matrigel) compared to migrate (thin matrigel) represents the invasion rate (% mean invasion). Invasion of the ZEB2 overexpression BeWo_c6 clone through a Matrigel-coated Transwell was significantly increased compared to BeWo_EV (Kruskal–Wallis test with Dunn’s multiple comparisons, $***P = 0.0007$), similar to the invasion rate of HTR8/SVneo ($****P < 0.0001$). JEG3 were analysed after 24-h migration/invasion. ZEB2 overexpressing JEG3_b5 clone invaded significantly faster compared to JEG3_EV (Kruskal–Wallis test with Dunn’s multiple comparisons, $*P = 0.02$). Results are the mean \pm SEM of three independent experiments performed in triplicate.

(5% FBS + EGF) at the centre of the disc, the invasion rate is captured by phase-contrast microscopy every 2 days for up to 8 days (Fig. 5B). The invasion of EV and ZEB2^{oe} clones was measured by 3D-BPM and expressed as an invasion rate (μ m/day). The BeWo_c6 clone invaded 2-fold faster through the ECM of the 3D-BPM, compared to control (BeWo_EV, $12.4 \pm 0.9 \mu$ m/day; BeWo_c6, $23.3 \pm 0.9 \mu$ m/day; $P = 0.0002$; Fig. 5C). In a similar manner, the JEG3_b5 clone invasion was faster compared to the control (JEG3_EV, $5.1 \pm 0.2 \mu$ m/day; JEG3_b5, $17.8 \pm 0.2 \mu$ m/day; $P < 0.0001$; Fig. 5C). These results are consistent with the Transwell assays described above.

The third measure of functionality employed real-time monitoring of invasion using the xCELLigence RTCA system, an electronically-integrated Boyden chamber. Similar to the Transwell assay, cells with invasive properties that are seeded on top of Matrigel degrade the ECM and travel towards a chemoattractant in a lower chamber. However, in the xCELLigence system, when the cells pass through the ECM, they adhere to the gold impedance electrodes and cause an increase in the electrical impedance signal (given as cell index). Using

this system, we tested two aspects of invasion related to ZEB2 overexpression. The first was confirmation of the differences between the ZEB2^{oe} clones and their respective EV controls. The results are shown in Fig. 6A and B, where the increased invasion rates of the BeWo_c6 and JEG3_b5 compared to EV controls are apparent.

In the 3D-BPM assay, the cells bioprinted at the periphery invade towards the centre of the disc, up a gradient of EGF. We used the xCELLigence assay to determine whether the invasion results observed in the 3D-BPM model were the result of EGF acting to modify the intrinsic invasiveness of the cells, rather than a chemotactic effect. Thus, all the cell invasion measurements using the xCELLigence system (both EV controls and ZEB2^{oe} clones) and shown in Fig. 6 were performed in the presence of 10 μ M EGF. It is clear from these measurements that the invasion rates for the ZEB2^{oe} clones are significantly greater than the EV controls (both performed in the presence of EGF). This demonstrates that the higher invasion rates of the ZEB2^{oe} clones are not the result of EGF modulation of cell function and validates the 3D-BPM measurements.

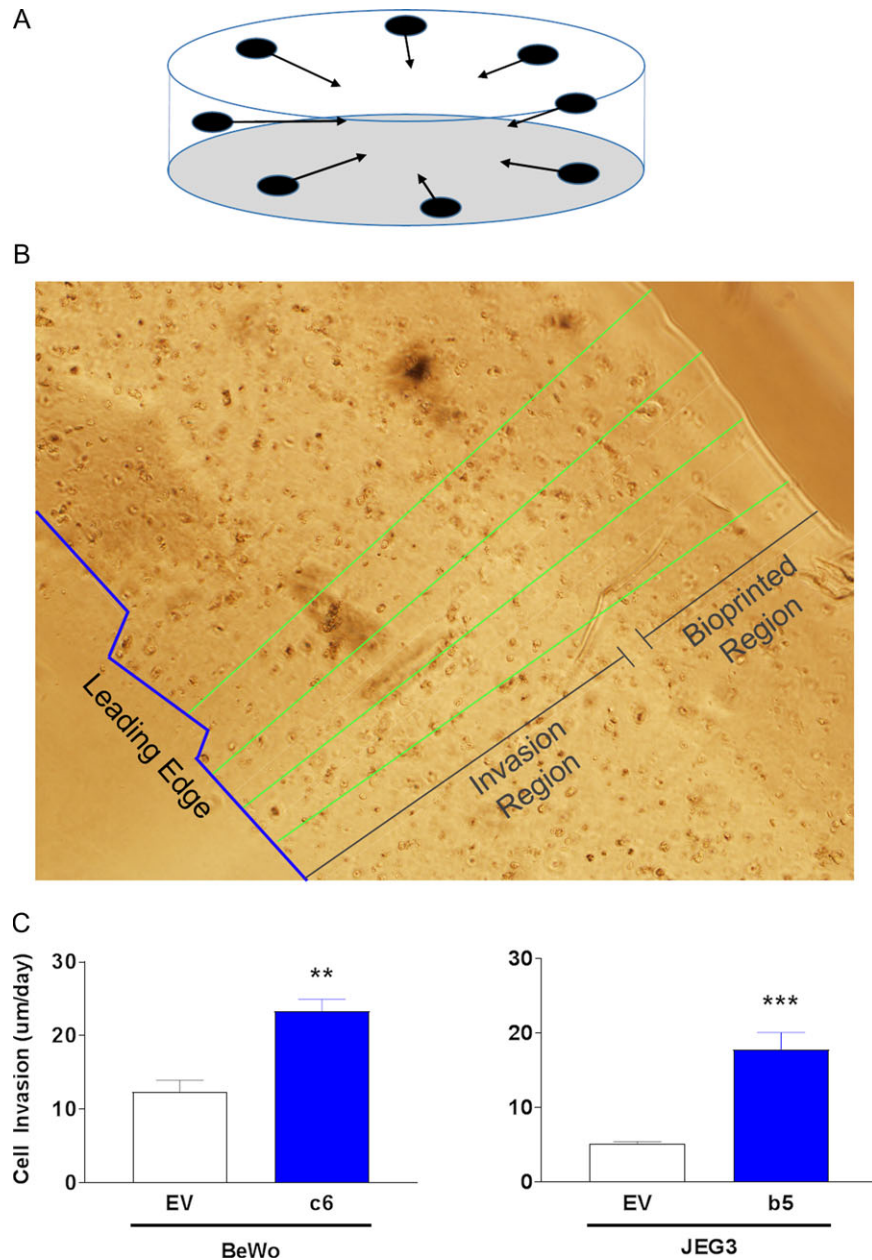


Figure 5 ZEB2 overexpression in trophoblast cell lines results in increased invasion in a 3D-Bioprinted Placental Model (3DBPM). A novel 3DBPM was used to assess invasion of BeWo and JEG3 clones (empty vector; EV or ZEB2 overexpression). (A) Cell invasion of BeWo and JEG3 choriocarcinoma cells was initiated by printing a shell of cells in the periphery of a gelMA hydrogel (extracellular matrix). (B) Cell invasion was measured as the cells travelled towards the centre of the construct towards a chemoattractant. Distance travelled was measured from the periphery to the leading edge and expressed as μm travelled/day. (C) Both BeWo_c6 and JEG3_b5 (ZEB2 overexpressing clones) had significantly augmented invasion compared to each cell line's respective EV (ANOVA with Tukey's multiple comparisons, *** $P = 0.0002$, **** $P < 0.0001$). Results are the mean \pm SEM performed in triplicate.

Protein expression in the stable ZEB2^{oe} clones

In addition to gene expression changes, we also examined a select series of proteins to determine whether the alterations in the ZEB2^{oe} clones' gene expression were reflected as changes in protein expression. These measurements were performed by immunofluorescence

and western blotting of clone cell lysates ($n = 3$ for all groups). In Supplementary Fig. 1A, E-cadherin fluorescent staining appears reduced in the BeWo_c6 clones that have pulled away from the cell colony. The results in Fig. 7 (and Supplementary Figs 2 and 3) compare protein expression by western blot in the parental cells, the EV controls and the ZEB2^{oe} clones. In Fig. 7A (and Supplementary Fig. 2), the data for BeWo shows that cytokeratins 7 and 14 are unchanged across

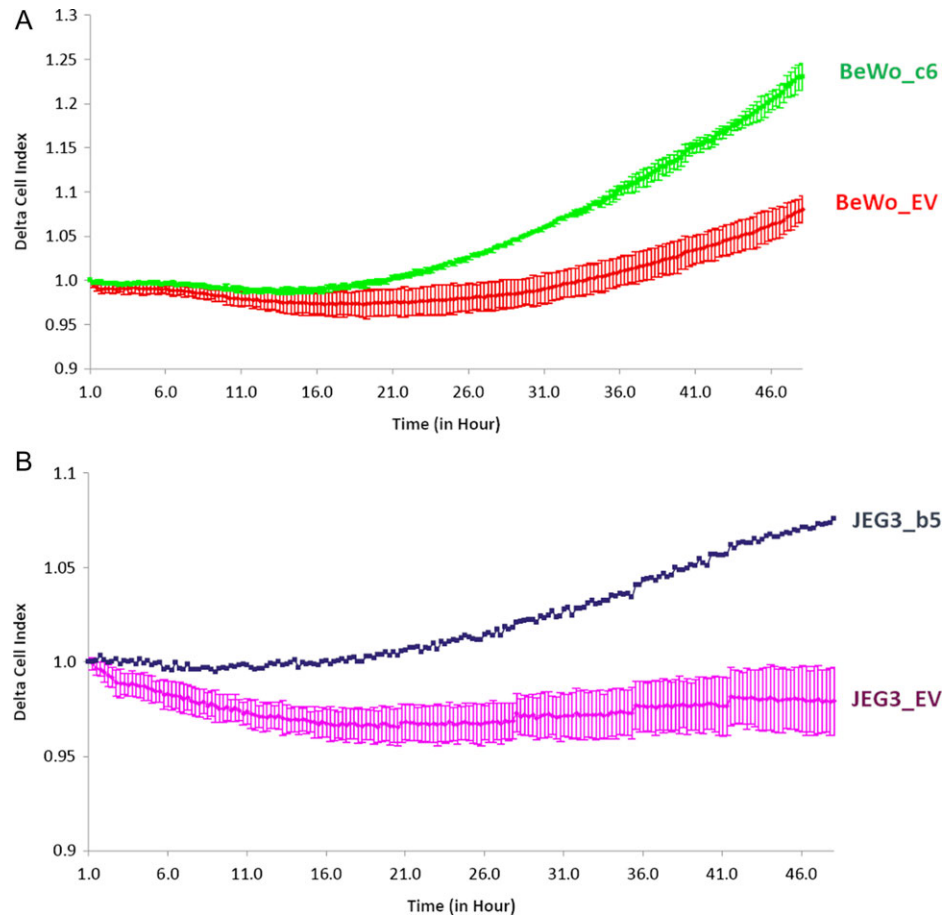


Figure 6 ZEB2 overexpression in trophoblast cell lines results in increased invasion in real-time. Both BeWo and JEG3 clones (empty vector; EV or ZEB2 overexpression) were assessed by the xCELLigence™ RTCA. Cell invasion of (A) BeWo and (B) JEG3 choriocarcinoma cells was captured in real-time as cells pass through Matrigel towards a chemoattractant. All experiments contained 10 μ M EGF. The graphs represent the delta cell index from at least four wells \pm SD.

the array of cells (BeWo_par, BeWo_EV, BeWo_f11, BeWo_c6), despite demonstrating significant increase in gene expression in the BeWo_c6 clone. The levels of other well-recognized EMT-associated proteins such as MMP-2, MMP-9, fibronectin, vimentin and IGFBP4 in BeWo_c6 are increased compared to the BeWo_EV control ($P < 0.05$; ANOVA; Fig. 7A). In the JEG3 cells, there are no significant changes in protein expression between the groups (JEG3_par, JEG3_EV, JEG3_a7, JEG3_b5; Fig. 7B, Supplementary Fig. 3). In Supplementary Fig. 1B, JEG3_b5 cells show no depreciable change in *OCLN* gene expression, yet the occludin tight junctions appear as punctate staining.

Discussion

Our goal was to overexpress ZEB2 in cultured trophoblast cell models to support or refute the hypothesis that the CTB to EVT transition is regulated by ZEB2, an EMT master regulatory transcription factor. We predicted that ZEB2 overexpression in BeWo and JEG3 would induce changes in gene expression and phenotypic alterations consistent with an EMT. Both BeWo and JEG3 were stably transduced with a lentiviral

vector coding for ZEB2. Two stable clones of each cell line were analysed for gene expression, protein and functional alterations, compared to EV controls. A targeted analysis of gene expression by an EMT-specific array confirmed differential expression in those ZEB2^{oe} clones, indicative of a shift towards a mesenchymal genotype. ZEB2 has been shown to be a promoter of invasion in malignant epithelial tumours following conditional upregulation (Comijn *et al.*, 2001; Vandewalle *et al.*, 2009). Therefore, successful ZEB2 overexpression in BeWo and JEG3 might be expected to promote cell invasiveness. We showed that the clones with increased ZEB2 protein exhibited substantial increases in invasiveness in multiple functional assays, including a Transwell endpoint assay, and two kinetic assays, a novel 3D-bioprinted placental model (3DBPM) and the xCELLigence system. Thus, the evidence for an EMT comprises (1) multiple changes in gene expression, the majority of which reflect an epithelial–mesenchymal shift, (2) changes in cell morphology, (3) changes in protein expression and (4) most importantly, substantial increases in invasiveness in the high ZEB2^{oe} clones. While loss of invasiveness is easy to induce through the alterations in a single system, increases are important because they imply multiple, coordinated alterations in cell systems

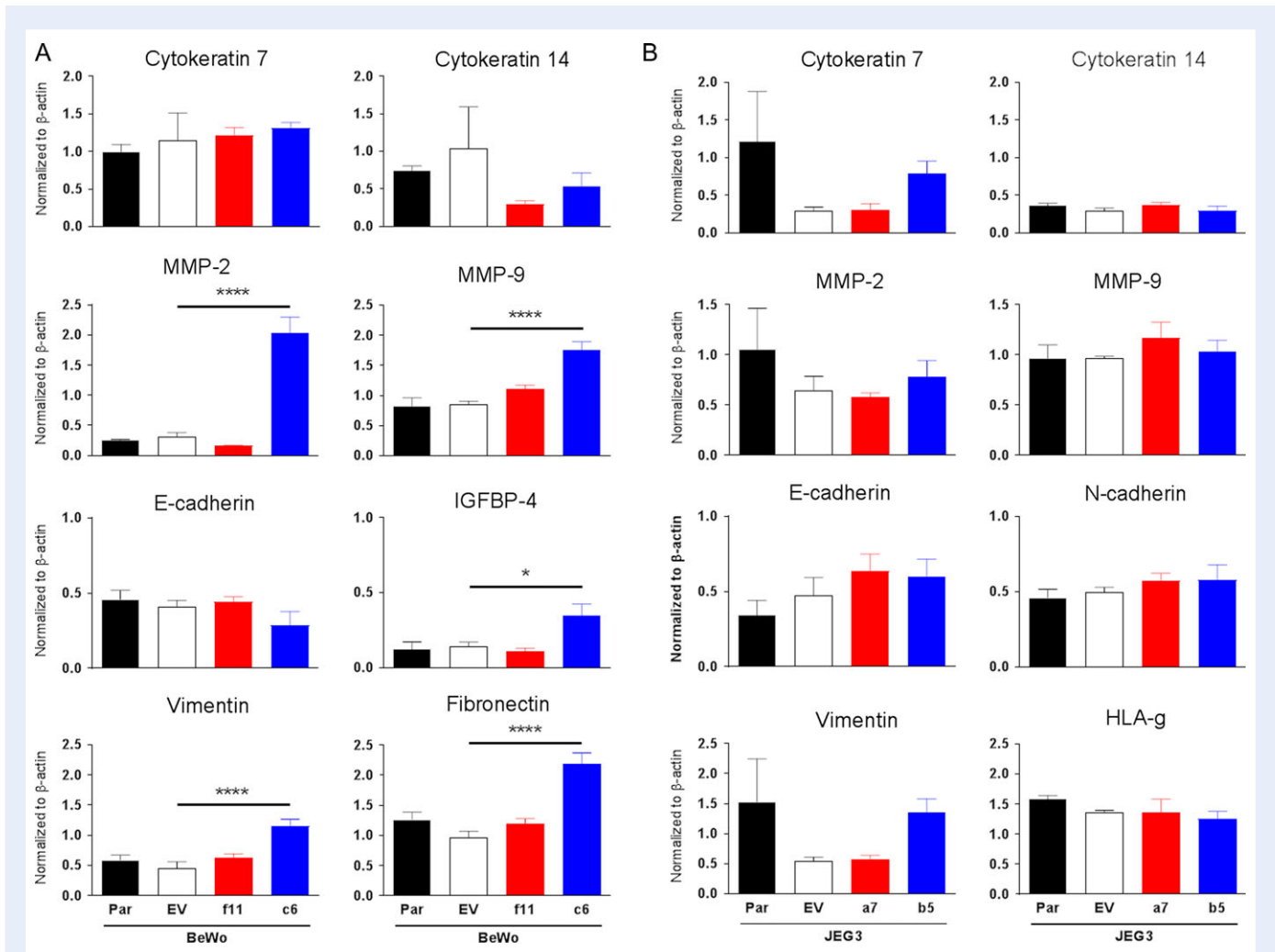


Figure 7 Protein expression changes in *ZEB2* overexpressing BeWo and JEG3 clones. The protein expression of all cell lines (parental; Par, empty vector; EV or *ZEB2* overexpression) was analysed by western immunoblot. The results were quantified and normalized to β -actin. **(A)** The BeWo_c6 clone has increased expression of mesenchymal-associated markers including matrix metalloproteinases (MMP2 and MMP9), vimentin and fibronectin compared to controls (BeWo_Par and BeWo_EV; ANOVA with Tukey's multiple comparisons, $*P = 0.04$, $****P < 0.0001$). **(B)** The protein expression of JEG3 cells was not significantly different from control. Results are the mean \pm SD analysed in triplicate.

which are necessary to increase invasiveness. We conclude that our hypothesis, that *ZEB2* expression promotes alterations consistent with an epithelial–mesenchymal transition coupled with increased invasiveness, is supported.

While all the clones selected for downstream analyses had mesenchymal features, only BeWo_c6 and JEG3_b5 showed increased *ZEB2* protein, and only BeWo_c6 and JEG3_b5 displayed increased invasiveness in the Transwell assays. The disparity between the levels of *ZEB2* gene overexpression and the small increases in *ZEB2* protein is explained by a recent finding which shows that a section of the *ZEB2* mRNA induces ribosomal pausing and compromises protein synthesis (Wan Makhtar et al., 2017). This protein-coding section requires stretches of rare codons which leads to restricted protein synthesis. Thus, *ZEB2* protein is only achievable at higher levels of *ZEB2* mRNA expression.

BeWo_c6 expresses a well-recognized pattern of gene up- and down-regulation consistent with an EMT. These include the decrease in the expression of genes associated with cell–cell junctions and cell–

cell adhesion (*DSP*, *F11R*, *OCLN*, *PLEK2*) and the gain in matrix metalloproteinases (*MMP2*, *MMP9*). However, JEG3_b5 displays a different set of changes, many associated with EMT, including upregulation of *CDH2*, *GSK3B*, *ITGA5* and *SNAI2*. In addition, both BeWo_c6 and JEG3_b5 also demonstrate gene expression changes that are dissimilar to the patterns seen in Types 1–3 EMT (Kalluri and Weinberg, 2009; Thiery et al., 2009). These observations raise important points. The first is that limiting classification to the Type 1–3 definitions is too restrictive; even within these classifications there are numerous differences and deviations. As we have noted previously, cytotrophoblast differentiation is likely a different form of EMT (DaSilva-Arnold et al., 2015, 2018). The use of the PCR array has enabled us to examine a wide range of markers, however appropriate identification should also require functional measures, such as the demonstration of altered invasiveness described here.

Other aspects of the clones' differential gene expression are worth noting. Unlike the BeWo *ZEB2*^{oe} clones, the JEG3 *ZEB2*^{oe} clones show

significant changes in several other EMT master regulatory transcription factors (decreased *SNAI1*, increased *SNAI2* and *TWIST1*) as a result of *ZEB2* overexpression. There is clear evidence from the other EMT types of a variety of combinations of regulatory pathways which result in EMT (Peinado *et al.*, 2007; Thiery *et al.*, 2009; Tania *et al.*, 2014; Pattabiraman and Weinberg, 2016). The fact that the JEG3_b5 also showed increased *ZEB2* protein, altered morphology and increased invasiveness suggests that cell-specific alternate regulatory pathways, downstream of *ZEB2*, may result in the same EMT-related endpoints. The differences in gene expression patterns between BeWo_c6 and JEG3_b5 may reflect the inherent phenotypic differences between these two choriocarcinoma cell lines. While some changes in the JEG3_b5 clone are expected, such as the significant gain in neural (N)-cadherin (*CDH2*), a molecule present in highly motile cells, others are not. One example is a hallmark feature of the EMT, the down-regulation of (E)-cadherin (*CDH1*). Instead we saw significant gain in *CDH1* expression in our JEG3_b5 clone, but it did not translate into increased protein production. This is perhaps because sumoylation of *ZEB2* reduces its ability to transcriptionally suppress *CDH1* without any effect on *ZEB2* subcellular localization. Therefore, the loss of *CDH1* is attenuated even with ample *ZEB2* upregulation (Long *et al.*, 2005).

Previous microarray studies showed that ~2700 genes were differentially expressed between the BeWo and JEG3 choriocarcinoma lines, suggesting major differences in cell adhesion, signal transduction and protein metabolism possibly related to differences in lineage (Burleigh *et al.*, 2007). The parental JEG3 are more invasive and express HLA-G, a marker for extravillous trophoblast (Lala *et al.*, 2002), suggesting they may already be further along the EMT than the BeWo. It is also possible that these patterns may indicate that *ZEB2* stimulates alternate pathways in these two cell types, acting in a redundant manner to yield the same end-results, i.e. loss of cell–cell adhesion, loss of cell polarity and increased invasive capacity. That both BeWo_c6 and JEG3_b5 demonstrate an EMT is shown not only by the multiple gene expression changes consistent with an EMT, but also by the increased invasiveness and morphologic alterations consistent with loss of cell–cell adhesion and polarity. If we accept that both clones undergo an EMT as a result of *ZEB2* overexpression, then we can conclude that the same endpoint, EMT, may be achieved via alternate pathways.

The other notable observation concerns the cytokeratins. Theoretically, cells require transcription factor signalling alterations, polarity changes and cytoskeletal remodelling for a complete progression of the EMT. Yet, some cells transiently express features of a partial EMT state (Lee *et al.*, 2006; Yang and Weinberg, 2008; Lim and Thiery, 2012). Recent observations suggest that cells undergoing EMT are not only capable of displaying a spectrum of epithelial/mesenchymal phenotypes but may also possess alternate pathways for activation (Pattabiraman and Weinberg, 2016; Jolly *et al.*, 2017). Trophoblast cells may also be capable of a partial EMT, in which they simultaneously retain epithelial markers while gaining mesenchymal traits. In this manner, cells may have a degree of plasticity, maintaining the ability to progress towards a mesenchymal state or revert back to an epithelial state, often defined as a ‘metastable’ state (Lee *et al.*, 2006; Jordan *et al.*, 2011; Tam and Weinberg, 2013). As trophoblast cells undergo the EMT, they appear to retain epithelial cytokeratins which would be expected to be suppressed in a more complete EMT.

The key element supporting an EMT in BeWo_c6 and JEG3_b5 is that *ZEB2* overexpression results in a significant functional change, e.g. increased invasive behaviour, demonstrated across all platforms. We first tested the clones in a widely used and reliable measure of invasion, the Transwell Matrigel assay, where both the BeWo_c6 and JEG3_b5 clones easily traversed an extracellular matrix barrier (ECM; Matrigel). These clones were also analysed in 3D using a novel placental bioprinted model (3D-BPM), a system that mimics the *in-vivo* 3D structure and dimensionality of the placenta while permitting real-time data acquisition. With these advantages, we were able to provide a robust alternate measurement of trophoblast invasion, generating results consistent with the Transwell assays. In the xCELLigence system, similar to the previous two invasion measures, the BeWo_c6 and JEG3_b5 showed substantial increases in invasive capacity compared to the EV controls, as measured by the increase in electrical impedance occurring as cells traversed the ECM. It has been suggested that EGF acts as an EMT inducer through *TWIST1* upregulation resulting in a decrease of *CDH1* and an increase in *VIM* production (Lo *et al.*, 2007). Since our invasion studies in the 3D-BPM used EGF as a chemo-attractant, we sought to verify that this ligand was not responsible directly for increased invasiveness. We therefore used the xCELLigence system to test whether EGF was acting as a promoter of EMT. Despite the fact that EGF was present in both experimental (BeWo_c6, JEG3_b5) and control (BeWo_EV, JEG3_EV) groups, both experimental clones showed substantial invasive capacity compared to the EV controls, demonstrating that EGF was not responsible for the augmented invasive capacity.

There is broad correlation between the data obtained from the different invasion models, in that only those clones with upregulation of *ZEB2* sufficient to increase ZEB protein levels have an enhanced invasive phenotype. In the case of BeWo_f11, for example, despite the increase in a classical mesenchymal marker like *VIM* (vimentin), there is no functional change in invasion at the lower level of *ZEB2* upregulation. We surmise that there is a basal level of *ZEB2* overexpression that must be achieved to enable translation of sufficient *ZEB2* protein to enable activation of the EMT, resulting in increased invasiveness. These results indicate also that despite pattern variations in gene and protein expression between BeWo_c6 and JEG3_b5, *ZEB2* manipulation yields a substantial shift in function (e.g. increased invasion). This demonstration of a change in functionality is central to the definition of the EMT process. Loss of functionality, through manipulation of the complex systems which make up the differentiation process, is a common experimental observation in many studies. This does not however indicate that the altered component is regulatory, simply that it is necessary for function. Our demonstration of increased functionality is important since it suggests that *ZEB2* is coordinating the multiple systems necessary to promote invasion, with activation of differing pathways towards that functional goal, as revealed by comparison between model cell lines.

Investigating the role of *ZEB2 in-vitro*, in cultured model cell lines, may be considered a limitation in our studies, however we believe these trophoblast model cell experiments are crucial to our exploration of the CTB differentiation mechanism. Unlike primary cells, these cells are proliferative, allowing development of stable clones for extended investigation. As part of the experimental design, we purposely employed two different trophoblast model lines to ensure that the effects of manipulation were not cell type-specific. The results

here provide a framework for experimentation on primary cells. However, overexpression techniques permitting a reliable generation of sufficient, healthy, transduced primary cells for assays of invasiveness are not yet available.

We conclude from the data reported here that *ZEB2* stimulates a trophoblast EMT in both BeWo and JEG3 cells. The EMT is defined not only by changes in gene expression but also in protein expression, morphology and invasive capacity. The data from this gain-of-function experiment is consistent with our prior *in-vivo* data in which high levels of *ZEB2* expression in first trimester trophoblast were associated with invasive EVT, and reduced levels of invasive capacity in the third trimester correlated with low levels of *ZEB2*. This is also reflected in the invasive EVT model cell line, HTR8/SVneo; these cells were found in a microarray study to share ~1188 transcripts with primary EVT and therefore, serve as a model for epithelial biology and extravillous trophoblast cell invasion (Bilban et al., 2010). Our data shows that the expression of *ZEB2* in HTR8/SVneo was ~40-fold greater, as measured by PCR array, than BeWo and JEG3 parent and EV controls. Both *in-vivo* and *in-vitro*, other EMT-associated master regulatory transcription factors (e.g. *GSC*, *SNAI1*, *SNAI2*, *TWIST1*, *ZEB1*) fail to demonstrate the relationship between expression and EVT invasiveness displayed by *ZEB2*, arguing for the key role of the latter as the primary regulator of CTB differentiation to EVT, mediated via the EMT mechanism. These results serve as a foundation for more targeted studies of invasion *in-vivo* and of the elements which regulate differentiation and invasive capacity. In depth studies of the differentiation mechanisms *in-vivo* will also enable us to derive diagnostic indicators of abnormal invasion and, potentially, to develop the therapeutic manoeuvres necessary to correct problems arising from aberrant differentiation.

Supplementary data

Supplementary data are available at *Molecular Human Reproduction* online.

Acknowledgements

The authors wish to thank the staff at the New Jersey Medical Flow Cytometry Core specifically Sukhwinder Singh and Tammy Mui for their expertise. We also thank Dr Charles Graham at Queen's University for his generous gift of HTR-8/SVneo, Dr William Ackerman III at The Ohio State University for his generous gift of JEG3, and Dr Kenneth Audus at the University of Kansas for his generous gift of BeWo.

Authors' roles

Experiments were conceived and designed by SDA, NPI, SZ and AA. Invasion assays were carried out by SDA, CK, VD and YR. SDA, CK, VD and NPI performed the experimental analyses and data collection. PCK, JPF and RB contributed materials. SDA, SZ and NPI carried out the data interpretation. The manuscript was written by SDA and edited by NPI, SZ, CK, VD and AA. Manuscript was approved for submission by all authors.

Funding

Funding was provided by the Department of Obstetrics and Gynecology, Division of Maternal-Fetal Medicine and Surgery at

Hackensack Meridian Health, Hackensack, NJ. The 3D bioprinted placental model studies performed in Dr. Kim's and Fisher's laboratories were supported by the Children's National Medical Center. The xCELLigence work performed in Dr. Birge's laboratory was supported by NIH CA165077.

Conflict of Interest

The authors declare no competing financial interests.

References

- Bilban M, Tauber S, Haslinger P, Pollheimer J, Saleh L, Pehamberger H, Wagner O, Knofler M. Trophoblast invasion: assessment of cellular models using gene expression signatures. *Placenta* 2010;**31**:989–996.
- Buijs JT, Henriquez NV, van Overveld P G, van der Horst G, ten Dijke P, van der Pluijm G. TGF-beta and BMP7 interactions in tumour progression and bone metastasis. *Clin Exp Metastasis* 2007;**24**:609–617.
- Burleigh DW, Kendziorski CM, Choi YJ, Grindle KM, Grendell RL, Magness RR, Golos TG. Microarray analysis of BeWo and JEG3 trophoblast cell lines: identification of differentially expressed transcripts. *Placenta* 2007;**28**:383–389.
- Comijn J, Berx G, Vermassen P, Verschuere K, van Grunsven L, Bruyneel E, Mareel M, Huylebroeck D, van Roy F. The two-handed E box binding zinc finger protein SIP1 downregulates E-cadherin and induces invasion. *Mol Cell* 2001;**7**:1267–1278.
- DaSilva-Arnold S, James JL, Al-Khan A, Zamudio S, Illsley NP. Differentiation of first trimester cytotrophoblast to extravillous trophoblast involves an epithelial-mesenchymal transition. *Placenta* 2015;**36**:1412–1418.
- DaSilva-Arnold S, Zamudio S, Al-Khan A, Alvarez-Perez J, Mannion C, Koenig C, Luke D, Perez A, Petroff M, Alvarez M et al. Human trophoblast epithelial-mesenchymal transition in abnormally invasive placenta. *Biol Reprod* 2018;**99**:409–421.
- Duangkumpha K, Techasen A, Loilome W, Namwat N, Thanan R, Khuntikeo N, Yongvanit P. BMP-7 blocks the effects of TGF-beta-induced EMT in cholangiocarcinoma. *Tumour Biol* 2014;**35**:9667–9676.
- Eger A, Aigner K, Sonderegger S, Dampier B, Oehler S, Schreiber M, Berx G, Cano A, Beug H, Foisner R. DeltaEF1 is a transcriptional repressor of E-cadherin and regulates epithelial plasticity in breast cancer cells. *Oncogene* 2005;**24**:2375–2385.
- Greenburg G, Hay ED. Epithelia suspended in collagen gels can lose polarity and express characteristics of migrating mesenchymal cells. *J Cell Biol* 1982;**95**:333–339.
- Jolly MK, Ware KE, Gilja S, Somarelli JA, Levine H. EMT and MET: necessary or permissive for metastasis? *Mol Oncol* 2017;**11**:755–769.
- Jordan NV, Johnson GL, Abell AN. Tracking the intermediate stages of epithelial-mesenchymal transition in epithelial stem cells and cancer. *Cell Cycle* 2011;**10**:2865–2873.
- Justus CR, Leffler N, Ruiz-Echevarria M, Yang LV. In vitro cell migration and invasion assays. *J Vis Exp* 2014:10–24.
- Kalluri R, Weinberg RA. The basics of epithelial-mesenchymal transition. *J Clin Invest* 2009;**119**:1420–1428.
- Khong TY, Robertson WB. Placenta creta and placenta praevia creta. *Placenta* 1987;**8**:399–409.
- Kokkinos MI, Murthi P, Wafai R, Thompson EW, Newgreen DF. Cadherins in the human placenta—epithelial-mesenchymal transition (EMT) and placental development. *Placenta* 2010;**31**:747–755.
- Kuo CY, Eranki A, Placone JK, Rhodes KR, Aranda-Espinoza H, Fernandes R, Fisher JP, Kim PC. Development of a 3D printed, bioengineered

- placenta model to evaluate the role of trophoblast migration in pre-eclampsia. *ACS Biomater Sci Eng* 2016;**2**:9.
- Kuo CY, Guo T, Cabrera-Luque J, Arumugasaamy N, Bracaglia L, Garcia-Vivas A, Santoro M, Baker H, Fisher J, Kim P. Placental basement membrane proteins are required for effective cytotrophoblast invasion in a three-dimensional bioprinted placenta model. *J Biomed Mater Res A* 2018a;**106**:1476–1487.
- Kuo CY, Wilson E, Fuson A, Gandhi N, Monfaredi R, Jenkins A, Romero M, Santoro M, Fisher JP, Cleary K et al. Repair of tympanic membrane perforations with customized bioprinted ear grafts using Chinchilla models. *Tissue Eng Part A* 2018b;**24**:527–535.
- Lala PK, Lee BP, Xu G, Chakraborty C. Human placental trophoblast as an in vitro model for tumor progression. *Can J Physiol Pharmacol* 2002;**80**:142–149.
- Lee JM, Dedhar S, Kalluri R, Thompson EW. The epithelial-mesenchymal transition: new insights in signaling, development, and disease. *J Cell Biol* 2006;**172**:973–981.
- Lim J, Thiery JP. Epithelial-mesenchymal transitions: insights from development. *Development* 2012;**139**:3471–3486.
- Livak KJ, Schmittgen TD. Analysis of relative gene expression data using real-time quantitative PCR and the 2(-Delta Delta C(T)) Method. *Methods* 2001;**25**:402–408.
- Lo HW, Hsu SC, Xia W, Cao X, Shih JY, Wei Y, Abbruzzese JL, Hortobagyi GN, Hung MC. Epidermal growth factor receptor cooperates with signal transducer and activator of transcription 3 to induce epithelial-mesenchymal transition in cancer cells via up-regulation of TWIST gene expression. *Cancer Res* 2007;**67**:9066–9076.
- Long J, Zuo D, Park M. Pc2-mediated sumoylation of Smad-interacting protein 1 attenuates transcriptional repression of E-cadherin. *J Biol Chem* 2005;**280**:35477–35489.
- Lyden TW, Ng AK, Rote NS. Modulation of phosphatidylserine epitope expression by BeWo cells during forskolin treatment. *Placenta* 1993;**14**:177–186.
- Naber HP, Wiercinska E, Pardali E, van Laar T, Nirmala E, Sundqvist A, van Dam H, van der Horst G, van der Pluijm G, Heckmann B et al. BMP-7 inhibits TGF-beta-induced invasion of breast cancer cells through inhibition of integrin beta(3) expression. *Cell Oncol (Dordr)* 2012;**35**:19–28.
- Naicker T, Khedun SM, Moodley J, Pijnenborg R. Quantitative analysis of trophoblast invasion in preeclampsia. *Acta obst et Gynecol Scand* 2003;**82**:722–729.
- Pattabiraman DR, Weinberg RA. Targeting the epithelial-to-mesenchymal transition: the case for differentiation-based therapy. *Cold Spring Harb Symp Quant Biol* 2016;**81**:11–19.
- Peinado H, Olmeda D, Cano A. Snail, Zeb and bHLH factors in tumour progression: an alliance against the epithelial phenotype? *Nat Rev Cancer* 2007;**7**:415–428.
- Pijnenborg R, Dixon G, Robertson WB, Brosens I. Trophoblastic invasion of human decidua from 8 to 18 weeks of pregnancy. *Placenta* 1980;**1**:3–19.
- Schroeder A, Mueller O, Stocker S, Salowsky R, Leiber M, Gassmann M, Lightfoot S, Menzel W, Granzow M, Ragg T. The RIN: an RNA integrity number for assigning integrity values to RNA measurements. *BMC Mol Biol* 2006;**7**:3.
- Tam WL, Weinberg RA. The epigenetics of epithelial-mesenchymal plasticity in cancer. *Nat Med* 2013;**19**:1438–1449.
- Tania M, Khan MA, Fu J. Epithelial to mesenchymal transition inducing transcription factors and metastatic cancer. *Tumour Biol* 2014;**35**:7335–7342.
- Tantbirojn P, Crum CP, Parast MM. Pathophysiology of placenta creta: the role of decidua and extravillous trophoblast. *Placenta* 2008;**29**:639–645.
- Thiery JP, Acloque H, Huang RY, Nieto MA. Epithelial-mesenchymal transitions in development and disease. *Cell* 2009;**139**:871–890.
- Vandewalle C, Van Roy F, Berx G. The role of the ZEB family of transcription factors in development and disease. *Cell Mol Life Sci* 2009;**66**:773–787.
- Vicovac L, Aplin JD. Epithelial-mesenchymal transition during trophoblast differentiation. *Acta Anat* 1996;**156**:202–216. (Basel).
- Wan Makhtar WR, Browne G, Karountzos A, Stevens C, Alghamdi Y, Bottrill AR, Mistry S, Smith E, Bushel M, Pringle JH et al. Short stretches of rare codons regulate translation of the transcription factor ZEB2 in cancer cells. *Oncogene* 2017;**36**:6640–6648.
- Yang J, Weinberg RA. Epithelial-mesenchymal transition: at the crossroads of development and tumor metastasis. *Dev Cell* 2008;**14**:818–829.
- Zeisberg M, Hanai J, Sugimoto H, Mammoto T, Charytan D, Strutz F, Kalluri R. BMP-7 counteracts TGF-beta I-induced epithelial-to-mesenchymal transition and reverses chronic renal injury. *Nat Med* 2003;**9**:964–968.